

Frequency-Domain Detection for Molecular Communication with Cross-Reactive Receptors

Meltem Civas, *Student Member, IEEE*, Murat Kuscü, *Member, IEEE*, and Ozgur B. Akan, *Fellow, IEEE*

Abstract—Molecular Communications (MC) is a bio-inspired communication paradigm that uses molecules as information carriers, requiring unconventional transceivers and modulation/detection techniques. Practical MC receivers (MC-Rxs) can be implemented using field-effect transistor biosensor (bioFET) architectures, where surface receptors reversibly react with ligands. The time-varying concentration of ligand-bound receptors is translated into electrical signals via field effect, which is used to decode the transmitted information. However, ligand-receptor interactions do not provide an ideal molecular selectivity, as similar ligand types, i.e., interferers, co-existing in the MC channel, can interact with the same type of receptors. Overcoming this molecular cross-talk in the time domain can be challenging, especially when Rx has no knowledge of the interferer statistics or operates near saturation. Therefore, we propose a frequency-domain detection (FDD) technique for bioFET-based MC-Rxs that exploits the difference in binding reaction rates of different ligand types reflected in the power spectrum of the ligand-receptor binding noise. We derive the bit error probability (BEP) of the FDD technique and demonstrate its effectiveness in decoding transmitted concentration signals under stochastic molecular interference compared to a widely used time-domain detection (TDD) technique. We then verified the analytical performance bounds of the FDD through a particle-based spatial stochastic simulator simulating reactions on the MC-Rx in microfluidic channels.

Index Terms—Molecular communications, receiver, frequency-domain detection, biosensor, ligand-receptor interactions.

I. INTRODUCTION

Using molecules to encode and transfer information, i.e., Molecular Communications (MC), is nature’s way of connecting *bio things*, such as natural cells, with each other. Engineering this unconventional communication paradigm extend our connectivity to synthetic *bio-nano things*, such as nanobiosensors, artificial cells, is the vision that gave rise to the Internet of Bio-Nano Things (IoBNT). IoBNT is a novel networking framework with potential to enable groundbreaking healthcare and environmental applications [1]–[4].

The authors are with the Department of Electrical and Electronics Engineering, Koç University, Istanbul, Turkey (e-mail: {mcivas16, mkuscü, akan}@ku.edu.tr).

Ozgur B. Akan is also with the Internet of Everything (IoE) Group, Electrical Engineering Division, Department of Engineering, University of Cambridge, Cambridge, CB3 0FA, UK (email: oba21@cam.ac.uk).

This work was supported in part by the AXA Research Fund (AXA Chair for Internet of Everything at Koç University), The Scientific and Technological Research Council of Turkey (TUBITAK) under Grant #120E301, European Union’s Horizon 2020 Research and Innovation Programme through the Marie Skłodowska-Curie Individual Fellowship under Grant Agreement #101028935, and Huawei Graduate Research Scholarship.

A preliminary version of this work was presented at IEEE International Conference on Communications (ICC) on June 2023.

MC is fundamentally different from conventional electromagnetic communication techniques as it requires novel transceiver architectures as well as new modulation, coding, and detection techniques that can cope with the highly time-varying, nonlinear, and complex channel characteristics in biochemical environments [5]. The design of MC receivers (MC-Rxs) and detection techniques has unquestionably attracted the most attention in the literature. However, due to the simplicity it provides in modeling, many of the previous studies considered passive Rx architectures, that are physically unlinked from the MC channel, and thus, of little practical relevance [5]. An emerging trend in MC is to model and design more practical MC-Rxs that employ ligand receptors on their surface as selective biorecognition units, resembling the sensing and communication interface of natural cells. One such design, which was practically implemented in [6], is based on field-effect transistor biosensors (bioFETs). In this design, ligand-receptor (LR) interactions are translated into electrical signals via field-effect for the decoding of the transmitted information.

LR interactions are fundamental to the sensing and communication of natural cells. However, the selectivity of biological receptors against their target ligands is not ideal, and this so-called receptor promiscuity results in cross-talk of other types of molecules co-existing in the biochemical environment [7], [8]. This cross-talk is often dealt with by natural cells through intracellular chemical reaction networks and multi-state receptor mechanisms, such as kinetic proofreading [9], [10]. The same molecular interference problem also applies to abiotic MC-Rxs using ligand receptors. However, the absence of such molecular mechanisms to mitigate interference makes imperative to develop reliable detection techniques for these systems.

In our previous studies on biosynthetic MC-Rxs, we addressed the molecular interference issue by developing time-domain detection techniques leveraging different ligand-receptor binding statistics [11] and channel sensing methods enabling simultaneous sensing of multiple ligand types, thereby allowing the mitigation of interference [9]. However, the techniques developed for biosynthetic MC-Rxs are not applicable to biosensor-based MC-Rxs as they rely on samples from the bound time intervals of individual receptors to differentiate between interferer and information molecules. In biosensor-based MC-Rxs, the time trajectories of individual receptor states are not accessible, as the received signal is based on the concentration of bound ligands, which is transduced into electrical signals with additional noise. The difficulty in decoding information from time-varying concentrations

of bound ligands is exacerbated, especially when the MC-Rx has no knowledge of the statistics of the interference concentration, and it operates near saturation. Therefore, new approaches are required to address the molecular interference issue for biosensor-based MC-Rxs.

In this paper, we introduce a novel frequency-domain detection (FDD) technique designed to address the challenge of distinguishing between different types of ligands for biosensor-based MC-Rxs. The FDD approach utilizes the power spectral density (PSD) of receptor occupancy fluctuations, i.e., binding noise, which contains the distinct characteristics of the different LR interactions. By leveraging this information, the FDD method enables the estimation of individual ligand concentrations in the channel.

Stochastic and reversible LR interactions can be represented through a one-step binding/unbinding model, where the state transition rates are determined by the binding and unbinding rates for the LR pair [12]. Although various types of ligands can interact with the same kind of receptors, these interactions often have different binding and unbinding rates. These differences in reaction rates are manifested in distinct characteristic frequencies f_c , which are also dependent on the concentrations of the involved ligands. The characteristic frequency of the LR pair appears as a cut-off frequency in the Lorentzian-shaped PSD of the binding noise. When multiple types of ligands interact with the receptors, the PSD can be represented as the superposition of the Lorentzian-shaped PSDs. In such a scenario, the characteristic frequencies that define the shape of the binding noise PSD contain information on both reaction rates and the concentrations of the different ligands. The proposed FDD method exploits this feature to estimate the concentration of information-carrying molecules. This estimation is realized with a quasi-maximum likelihood approach, specifically the Whittle likelihood, which is based on both the observed PSD and the model PSD of the electrical output fluctuations at the MC-Rx. This electrical signal incorporates the binding noise from which the concentration information is extracted. The FDD method optimally decodes the transmitted symbol based on the estimated information-carrying molecule concentration.

To our knowledge, the FDD method introduced in this work is a novel approach for biosensor-based MC-Rxs as it addresses the limitation of the existing TDD methods in distinguishing between information-carrying and interfering ligands. To quantify the performance of the FDD method, we derived bit error probability (BEP) in closed form and compared it with the BEP of the TDD method that uses a single sample from the electrical output of the MC-Rx for symbol detection. To validate the accuracy of our analytical results, we used a particle-based stochastic simulator, which allowed us to simulate LR interactions on the surface of the MC-Rx in a microfluidic channel, along with Monte Carlo simulations. Although FDD requires additional computational resources compared to TDD, it is a promising detection strategy for biosensor-based MC-Rxs, especially in high-interference cases where TDD methods underperform significantly. In an earlier version of this work [13], we derived theoretical performance bounds, while in the current version, we validate the theoretical results using particle-based stochastic simulations and Monte

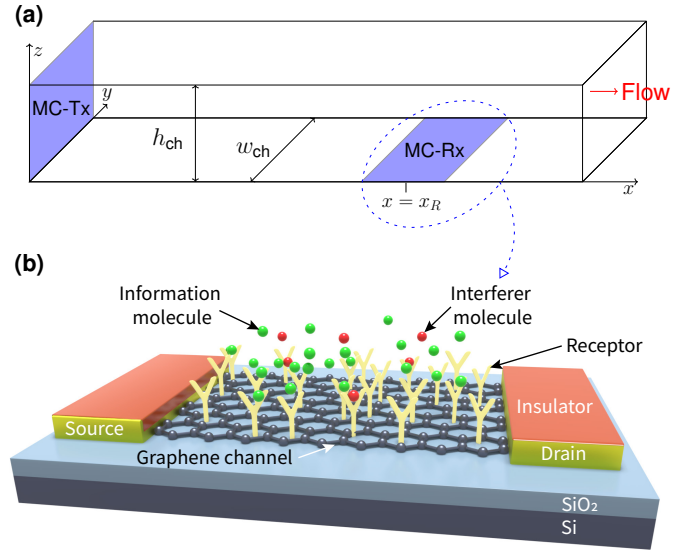


Fig. 1: A three-dimensional illustration (a) the microfluidic MC channel, including the positions of the MC-Tx and MC-Rx, and (b) the detailed view of the graphene bioFET-based MC-Rx exposed to information and interferer molecules.

Carlo experiments.

The rest of the paper is organized as follows. Section II provides an overview of the system model, while Section III details the TDD method. Next, Section IV introduces the FDD method. Section V outlines the validation procedure used to verify the theoretical derivations presented earlier. Following that, Section VI offers a comparative evaluation of the BEP performances of TDD and FDD methods. Finally, Section VII summarizes our conclusions.

II. SYSTEM MODEL

We consider an MC system that employs binary concentration shift keying (CSK). In this scenario, the transmitter (MC-Tx) emits $N_{m|s}$ information molecules at the beginning of each signaling interval. Here, m signifies the information-carrying molecules, while s , which can be either 0 or 1, denotes the transmitted bit. We assume that the signaling interval is long enough to neglect the effect of inter-symbol interference (ISI). The medium is a three-dimensional microfluidic channel with a rectangular cross-section, as illustrated in Fig. 1(a). The MC-Tx is located at the channel inlet, while the MC-Rx is positioned on the channel floor, centered at $x = x_R$. Molecules are released from the MC-Tx instantly and uniformly across the channel cross-section at the release time and propagate through a unidirectional fluid flow along the x -axis.

The MC-Rx is based on the graphene bioFET architecture, which uses graphene functionalized with uniform receptors as the transducer channel, as shown in Fig. 1(b). Graphene's unique electrical, mechanical, and biochemical properties, such as high charge carrier mobility, atomic thickness, and two-dimensional geometry combined with the bioFET configuration allowing signal amplification, enable highly sensitive detection of a wide range of biomolecules [14]. Graphene also

provides label-free detection as it allows the functionalization of its surface with biological probes that reversibly bind to the corresponding target. Recently, the first micro/nanoscale MC-Rx based on the graphene bioFET was demonstrated, using single-stranded DNA molecules as information carriers and their complementary strands as receptors on the graphene surface [6].

Information molecules can reversibly react with the receptors on the MC-Rx. Additionally, interferer molecules of a single type are present in the channel, and they can react with the MC-Rx receptors as well, albeit with differing reaction rates compared to the information molecules. The concentration of interferer molecules in the vicinity of the MC-Rx at the sampling time, denoted as c_i , is assumed to follow a log-normal distribution with a mean μ_{c_i} and variance $\sigma_{c_i}^2$. This statistical model is commonly employed for capturing the variability in biological systems [15].

Molecular propagation in the channel is governed by advection-diffusion processes. Given the instantaneous release of $N_{m|s}$ molecules from the MC-Tx, and under the assumption that receiver reactions negligibly affect the ligand concentration in the channel, the ligand concentration in the channel across space and time can be expressed as follows [16]:

$$c_{m|s}(x, t) = \frac{N_{m|s}}{A_{ch}\sqrt{4\pi Dt}} \exp\left(-\frac{(x-ut)^2}{4Dt}\right). \quad (1)$$

In (1), $A_{ch} = h_{ch}w_{ch}$ denotes the channel cross-sectional area, u represents the constant fluid flow velocity along the x -axis, and D is the effective diffusion coefficient. For channels having a rectangular cross-section, the effective diffusion coefficient D is formulated in relation to the intrinsic ligand diffusion coefficient D_0 , as follows [17]:

$$D = \left(1 + \frac{8.5u^2h_{ch}^2l_{ch}^2}{210D_0^2(h_{ch}^2 + 2.4h_{ch}l_{ch} + l_{ch}^2)}\right)D_0. \quad (2)$$

The peak of the ligand concentration profile reaches the MC-Rx's center position x_R at time $t_D = \frac{x_R}{u}$. Due to the low-pass filtering characteristics of the MC channel induced by the advection diffusion, the ligand concentration at the Rx position varies slowly. This allows the LR reactions to quickly reach equilibrium within a narrow time window centered around t_D [16], [17]. Within this temporal window, the MC-Rx can sample the receptor states, and the ligand concentration can be expressed as:

$$c_{m|s}(x_R, t_D) = \frac{N_{m|s}}{A_{ch}\sqrt{4\pi Dt_D}}. \quad (3)$$

Therefore, the probability of a single receptor being in a bound state in the presence of two different ligand types—information molecules and interferer molecules—can be expressed by

$$p_{b|s} = \frac{c_{m|s}/K_{D_m} + c_i/K_{D_i}}{1 + c_{m|s}/K_{D_m} + c_i/K_{D_i}}, \quad (4)$$

where $K_{D_m} = k_m^-/k_m^+$ and $K_{D_i} = k_i^-/k_i^+$ are the dissociation constant of information and interferer molecules, respectively [9]. The total number of receptors in the bound state $N_{b|s}$ follows a Binomial distribution with the mean

$\mu_{N_{b|s}} = p_{b|s}N_r$ and variance $\sigma_{N_{b|s}}^2 = p_{b|s}(1-p_{b|s})N_r$ [18]. Here, N_r represents the total number of independent surface receptors.

The binding of charged ligands to the receptors results in an effective charge on the graphene channel via electric field-effect. This can be described by $Q_{Gr|s} = N_{b|s}q_{eff}N_{e^-}$. Here, N_{e^-} is number of free electrons per ligand molecules. q_{eff} represents the mean effective charge of a single electron in a bound ligand in the presence of ionic screening, namely, Debye screening. This can be expressed as $q_{eff} = q \times \exp\left(-\frac{r}{\lambda_D}\right)$. In this expression, q is the elementary charge, r is effective length of a surface receptor, and λ_D is the Debye length. The Debye length, λ_D , is expressed by $\lambda_D = \sqrt{\frac{\epsilon\kappa_B T}{2N_A q^2 c_{ion}}}$, where ϵ represents the permittivity of the medium, T is the temperature, κ_B stands for Boltzmann's constant, N_A is Avogadro's constant, and c_{ion} denotes the ionic concentration of the medium [18]. Accordingly, the mean surface potential due to the bound ligands can be expressed as

$$\Psi_{Gr|s} = \frac{Q_{Gr|s}}{C_G}, \quad (5)$$

where $C_G = \left(\frac{1}{C_{Gr}} + \frac{1}{C_Q}\right)^{-1}$ is the total gate capacitance of the bioFET. C_{Gr} is the electrical double-layer capacitance between the graphene and electrolyte channel and is defined by $C_{Gr} = A_{Gr}\epsilon/\lambda_D$. In this expression, A_{Gr} is the area of the graphene surface exposed to the electrolyte. Additionally, C_Q represents the quantum capacitance and is obtained as $C_Q = c_q \times A_{Gr}$, where c_q is the quantum capacitance of graphene per unit area [6].

The change in the output current resulting from bound molecules at equilibrium can be formulated as $\Delta I_{b|s} = g \times \Psi_{Gr|s}$, where g is the transconductance of the bioFET. For a large number of bound receptors, the number of bound receptors at the sampling time can be approximated as Gaussian-distributed [18], i.e., $N_{b|s} \sim \mathcal{N}(\mu_{N_{b|s}}, \sigma_{N_{b|s}}^2)$. Considering the linearity of the transduction process, the change in the output current because of bound molecules can also be approximated as following a Gaussian distribution. The mean and variance of this distribution are $\mu_{\Delta I_{b|s}} = \zeta\mu_{N_{b|s}}$ and $\sigma_{\Delta I_{b|s}}^2 = \zeta^2\sigma_{N_{b|s}}^2$, respectively. Here, ζ is defined as $\frac{q_{eff}N_{e^-}g}{C_G}$.

In low-dimensional semiconductor materials such as graphene, another factor adding to the variability in the overall output current is $1/f$ noise. According to the widely-used charge-noise model for graphene FETs [19], the power spectral density of $1/f$ noise is described by $S_f(f) = \frac{S_{f_{1Hz}}}{f^\beta}$, where $S_{f_{1Hz}}$ is the noise power at 1 Hz, and β is an empirically determined noise exponent with a typical range of $0.8 \leq \beta \leq 1.2$. As discussed in [18], $1/f$ noise can be approximated as white noise within physically relevant observation windows. Accordingly, the variance of $1/f$ noise can be formulated as

$$\sigma_f^2 = \int_0^{f_L} S_f(f_L) df + \int_{f_L}^{f_H} S_f(f) df, \quad (6)$$

where f_L represents the lower frequency limit of the observation window, below which the noise power is considered constant, and f_H is the upper frequency limit, beyond which

the noise power is considered negligible. As a result, the respective variance and mean of the total output current change are given by $\sigma_{\Delta I_s}^2 = \zeta^2 \sigma_{N_{b|s}}^2 + \sigma_f^2$, $\mu_{\Delta I_s} = \mu_{\Delta I_{b|s}}$.

III. TIME-DOMAIN DETECTION

We assume that Rx has the knowledge of the number of information molecules transmitted, $N_{m|s}$, and the binding/unbinding rates of information and interferer molecules. Since Rx has no knowledge of the interferer concentration statistics, it constructs the optimal ML decision threshold for TDD solely based on its knowledge of the received signal statistics corresponding to the transmitted concentration of information molecules [11]:

$$\gamma_{td} = \frac{1}{\sigma_{\Delta I_1}^2 - \sigma_{\Delta I_0}^2} \left(\sigma_{\Delta I_1}^2 \mu_{\Delta I_0} - \sigma_{\Delta I_0}^2 \mu_{\Delta I_1} + \sigma_{\Delta I_1} \sigma_{\Delta I_0} \times \sqrt{(\mu_{\Delta I_1} - \mu_{\Delta I_0})^2 + 2(\sigma_{\Delta I_1}^2 - \sigma_{\Delta I_0}^2) \ln(\sigma_{\Delta I_1} / \sigma_{\Delta I_0})} \right). \quad (7)$$

As Rx does not account for interference statistics in calculating γ_{td} , it uses the bound state probability corresponding to a single molecule case, namely, $p_{b|s} = \frac{c_{m|s}/K_{D_m}}{1 + c_{m|s}/K_{D_m}}$.

To derive the BEP for TDD, we first obtain the statistics of the receiver output. By applying the law of total expectation, we can express the mean number of bound receptors as follows:

$$\mu_{N_{b|s}} = \int_0^\infty N_r p_{b|s}(c_i) f(c_i) dc_i, \quad (8)$$

where $p_{b|s}(c_i) = \frac{c_{m|s}/K_{D_m} + c_i/K_{D_i}}{1 + c_{m|s}/K_{D_m} + c_i/K_{D_i}}$, and $f(\cdot)$ is the probability density function of log-normal distribution. Hence, the mean output current change due to bound molecules is

$$\mu_{\Delta I_s} = \zeta \int_0^\infty N_r p_{b|s}(c_i) f(c_i) dc_i. \quad (9)$$

Similarly, by applying the law of total variance, we obtain the variance of the current change as

$$\sigma_{\Delta I_s}^2 = \zeta^2 \left(\int_0^\infty (1 - p_{b|s}(c_i)) p_{b|s}(c_i) N_r f(c_i) dc_i + \int_0^\infty (p_{b|s}(c_i) N_r)^2 f(c_i) dc_i \right) - \mu_{\Delta I_s}^2 + \sigma_f^2. \quad (10)$$

Therefore, given the decision threshold γ_{td} , BEP for TDD can be expressed as follows [11]:

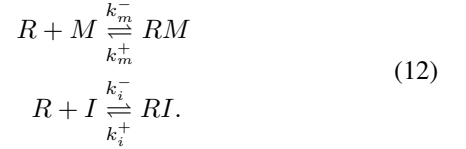
$$P_e^{TDD} = \frac{1}{4} \operatorname{erfc} \left(\frac{\gamma_{td} - \mu_{\Delta I_0}}{\sqrt{2\sigma_{\Delta I_0}^2}} \right) + \frac{1}{4} \operatorname{erfc} \left(\frac{\mu_{\Delta I_1} - \gamma_{td}}{\sqrt{2\sigma_{\Delta I_1}^2}} \right). \quad (11)$$

IV. FREQUENCY-DOMAIN DETECTION

In this section, we introduce the FDD method utilizing the model and observed PSD of the overall noise process (binding noise + $1/f$ noise of the graphene bioFET-based MC-Rx) to estimate the received concentration of information molecules c_m , which will be used in symbol decision. Here, the observed PSD is the periodogram of the noise constructed with the time-domain samples. In the sequel, we describe the model PSD and then introduce the proposed estimation method.

A. Theoretical Model of Binding Noise PSD

This section describes the theoretical model of the binding noise PSD for a particular pair of information and interference concentration, namely $\lambda = [c_m, c_i]$. The binding process of receptors can be described by the reaction model with three states, i.e., unbound (R), bound with information molecules (RM) and bound with interferer molecules (RI), with state occupation probabilities p_R, p_{RM} and p_{RI} , respectively [12]:



Hence, the chemical master equations are expressed as follows:

$$\begin{bmatrix} \frac{dp_{RM}}{dt} \\ \frac{dp_{RI}}{dt} \\ \frac{dp_R}{dt} \end{bmatrix} = \begin{bmatrix} -k_m^- & 0 & k_m^+ c_m \\ 0 & -k_i^- & k_i^+ c_i \\ k_m^- & k_i^- & -k_m^+ c_m - k_i^+ c_i \end{bmatrix} \begin{bmatrix} p_{RM} \\ p_{RI} \\ p_R \end{bmatrix} \quad (13)$$

The matrix containing reaction rates and the concentrations in (13), has rank 2 since one state probability can be written in terms of the other two state occupation probabilities as $p_R + p_{RM} + p_{RI} = 1$. Therefore, by setting the left-hand side in (13) to zero the equilibrium probabilities can be obtained as

$$p_{RM}^0 = \frac{c_m/K_{D_m}}{1 + \frac{c_m}{K_{D_m}} + \frac{c_i}{K_{D_i}}}, p_{RI}^0 = \frac{c_i/K_{D_i}}{1 + \frac{c_m}{K_{D_m}} + \frac{c_i}{K_{D_i}}} \quad (14)$$

and $p_R^0 = 1 - (p_{RM}^0 + p_{RI}^0)$. In the equilibrium conditions, the state occupation probabilities can be expressed in terms of the equilibrium state probability and the fluctuations around this probability [12], [20] as

$$p_j(t) = p_j^0 + \Delta p_j(t), \quad j \in \{RM, RI, R\}. \quad (15)$$

By substituting (15) into (13) and applying Taylor's expansion, the state fluctuations can be expressed as follows [12]:

$$\frac{d\Delta \mathbf{p}'(t)}{dt} = \mathbf{\Omega} \Delta \mathbf{p}'(t). \quad (16)$$

We define the column vector $\mathbf{p}(t)$ containing the state probabilities as $\mathbf{p}(t) = [p_{RM}(t), p_{RI}(t), p_R(t)]$ and its reduced form as $\mathbf{p}'(t) = [p_{RM}(t), p_{RI}(t)]$. Therefore, the relation between $\Delta \mathbf{p}'(t)$ and $\Delta \mathbf{p}(t)$ can be expressed as:

$$\Delta \mathbf{p}(t) = \mathbf{R} \Delta \mathbf{p}'(t), \quad (17)$$

where \mathbf{R} is the transformation matrix [12]. Also, the matrix $\mathbf{\Omega}$ in (16) is defined as follows:

$$\mathbf{\Omega} = \begin{bmatrix} -k_m^+ c_m - k_m^- & -k_m^+ \\ -k_i^+ c_i & -k_i^+ c_i - k_i^- \end{bmatrix}. \quad (18)$$

The deviation in the output current of the MC-Rx due to stochastic binding reactions, i.e., $\Delta I_b(t)$, is then obtained as

$$\Delta I_b(t) = \frac{q_{eff} g}{C_G} \mathbf{z}^T \mathbf{R} \Delta \mathbf{p}'(t) \quad (19)$$

where $\mathbf{z} = [N_{e-}; N_{e-}; 0]$ is the vector containing the number of elementary charges. As $\Delta I_b(t)$ is a stationary process,

the theoretical PSD of the binding noise fluctuations can be obtained by setting $t = 0$ as follows [12]:

$$\begin{aligned} S_b(f) &= 2 \mathcal{F}\{\mathbb{E}[\Delta I_b(t)\Delta I_b(t + \tau)]\} \\ &= 2 \mathcal{F}\{\mathbb{E}[\Delta I_b(0)\Delta I_b(\tau)]\} \\ &= 4N_r \left(\frac{q_{eff}g}{C_G}\right)^2 \mathbf{z}^T \mathbf{R} \Gamma (\text{Re}\{(j2\pi f \mathbf{I}_{2 \times 2} - \boldsymbol{\Omega})^{-1}\})^T \mathbf{R}^T \mathbf{z}, \end{aligned} \quad (20)$$

where $\mathcal{F}\{\cdot\}$ stands for Fourier transform, $\mathbf{I}_{2 \times 2}$ is the identity matrix, and Γ is the matrix containing the expected state probabilities, which is given as follows [12]:

$$\Gamma = \begin{bmatrix} p_{RM}^0 (1 - p_{RM}^0) & -p_{RM}^0 p_{RI}^0 \\ -p_{RM}^0 p_{RI}^0 & p_{RI}^0 (1 - p_{RI}^0) \end{bmatrix}. \quad (21)$$

Therefore, the theoretical PSD of the total current noise corresponding to a particular (c_m, c_i) pair can be written as

$$S(f) = S_b(f) + S_f(f). \quad (22)$$

B. Maximum Likelihood Estimation of PSD Parameters

In the following part, we describe the parameter value extraction, namely the estimation of information and interfering molecule concentrations, $\boldsymbol{\lambda} = [c_m, c_i]$, from the noise PSD. The detector uses the estimated information molecule concentration \hat{c}_m for symbol decision, as will be explained in the following section, Sec. IV-C. Our analysis is based on the following assumptions:

- The total noise process, namely the binding fluctuations combined with $1/f$ noise, is stationary, zero-mean with a single-sided spectrum.
- The MC-Rx is provided with the model PSD function, which is expressed by (22). MC-Rx also has the knowledge of the binding/unbinding rates of information and interferer molecules, and the number of information molecules transmitted for bits $s = 0$ and $s = 1$ as mentioned in Section II. Therefore, MC-Rx estimates the steady information and interferer concentrations by taking time samples from the output current ΔI_b in a sampling window, where we consider a single realization of the interferer concentration c_i following log-normal distribution as mentioned in Section II. The DC component of ΔI_b is discarded to isolate the noise.
- The information and interferer concentrations are considered constant in the sampling window based on the equilibrium assumption discussed in Section II [18].
- The observed PSD of time domain samples and the parametric model of the PSD expressed by (22) is used in the ML estimation of $\boldsymbol{\lambda} = [c_m, c_i]$. It is assumed that the observed PSD is calculated with the periodogram method.

For each transmitted symbol, we have N number of noise samples $\mathbf{x} = (x_1, x_2, \dots, x_N)$ taken with the sampling period of Δt . Hence, the total duration of sampling per symbol, namely the length of the sampling window, is $T_d = N\Delta t$. Periodogram for the sampled signal can be computed from the Discrete Fourier transform (DFT) of the samples \mathbf{x} . With even N , the periodogram values are then expressed as follows: $Y_k = \frac{2\Delta t}{N} |X_k|^2$ where $k = 1, \dots, N/2 - 1$, and $|X_k|$ are DFT components of \mathbf{x} .

For a stochastic time series of length N , the random variable $W_k = 2 \frac{Y_k}{S(f_k)}$ follows chi-squared distribution χ^2 [21], where $S(f_k)$, given by (22), is the true PSD at frequency f_k and $f_k = \frac{k}{N\Delta t}$ and $k = 1, \dots, N/2 - 1$. The χ^2 distribution with two degrees of freedom is in fact the exponential distribution [22]. Therefore, the periodogram values are exponentially distributed about the true PSD with the following probability given the model PSD value at a given frequency:

$$p(Y_k | S(f_k)) = \frac{1}{S(f_k)} e^{-\frac{Y_k}{S(f_k)}}, \quad (23)$$

following that $S(f_k)$ is also expectation value at f_k [22]. Based on (23), the likelihood of observing a pair of particular information and interferer concentrations, $\boldsymbol{\lambda} = [c_m, c_i]$, is

$$\mathcal{L}(\boldsymbol{\lambda}) = \prod_{k=1}^{N/2-1} p(Y_k | S(f_k, \boldsymbol{\lambda})) = \prod_{k=1}^{N/2-1} \frac{1}{S(f_k, \boldsymbol{\lambda})} e^{-\frac{Y_k}{S(f_k, \boldsymbol{\lambda})}}, \quad (24)$$

where $\boldsymbol{\lambda} = [c_m, c_i]$ is the parameters to be estimated. Here, we use Whittle likelihood, which can be a good approximation to the exact likelihood asymptotically, and also provide computational efficiency, i.e., $O(N \log N)$ computations compared to $O(N^2)$ for exact likelihood [22], [23]. Accordingly, the quasi-log likelihood can be written as follows:

$$\ln \mathcal{L}(\boldsymbol{\lambda}) = - \sum_{k=1}^{N/2-1} \left(\frac{Y_k}{S(f_k, \boldsymbol{\lambda})} + \ln S(f_k, \boldsymbol{\lambda}) \right). \quad (25)$$

ML estimator extracts the value of $\boldsymbol{\lambda}$, i.e., $\hat{\boldsymbol{\lambda}}$, that maximizes (25). Maximizing $\ln \mathcal{L}(\boldsymbol{\lambda})$ is equivalent to minimizing $l = -\ln \mathcal{L}(\boldsymbol{\lambda})$ [24], such that

$$\hat{\boldsymbol{\lambda}} = \arg \min_{\boldsymbol{\lambda}} \{l\}. \quad (26)$$

The solution to (26) can be obtained through numerical methods, such as the Newton-Raphson method achieving ML estimation in only a few iterations. The FDD method requires $O(N \log N)$ computations in addition to the numerical solution of (26). In the TDD approach, however, the MC-Rx takes a single time sample and performs a single thresholding operation to determine the received symbol.

C. Symbol Detection

The ML estimator described in Sec. IV-B is asymptotically unbiased such that $\hat{\boldsymbol{\lambda}}$ tends to have multi-normal distribution [25] with $\mathbb{E}[\hat{\boldsymbol{\lambda}}] = \boldsymbol{\lambda}$, and the respective variance of the estimated parameters, which is the diagonal elements of inverse Fisher information matrix (FIM) $\mathbf{F}(\boldsymbol{\lambda})$,

$$\sigma_{\hat{\lambda}_i}^2 = (\mathbf{F}(\boldsymbol{\lambda}))_{(ii)}^{-1}, \quad \mathbf{F}(\boldsymbol{\lambda})_{(ij)} = \mathbb{E} \left(\frac{\partial^2 l}{\partial \lambda_i \partial \lambda_j} \right). \quad (27)$$

where the expectation is taken with respect to the probability distribution of the observed spectrum $p(Y_1, Y_2, \dots, Y_N)$. Putting $l = -\ln \mathcal{L}(\boldsymbol{\lambda})$ into (27), the FIM can be expanded as:

$$\begin{aligned} \mathbf{F}_{(ij)} &= \\ &\mathbb{E} \left(\sum_{k=1}^{N/2-1} \frac{S(f_k) - Y_k}{S^2(f_k)} \frac{\partial^2 S}{\partial \lambda_i \partial \lambda_j} + \frac{2Y_k - S(f_k)}{S^3(f_k)} \frac{\partial S}{\partial \lambda_i} \frac{\partial S}{\partial \lambda_j} \right). \end{aligned} \quad (28)$$

Algorithm 1 Frequency Domain Detection

```

1: function FREQUENCYDETECTION( $Y[k], N, \Delta t, \gamma_{fd}$ )
2:   Find initial guess:  $\lambda^0 \leftarrow [c_m^0, c_i^0]$ 
3:    $f_k \leftarrow \frac{k}{N\Delta t}$  for  $k = 1, \dots, N/2 - 1$ 
4:   Use Newton's method on WHITTLE( $Y[k], f_k, \lambda$ ) with
   initial guess  $\lambda^0$  to find optimal  $\lambda^* = [c_m^*, c_i^*]$ .
5:    $\hat{c}_m \leftarrow c_m^*$ 
6:   if  $\hat{c}_m > \gamma_{fd}$ 
7:     Estimated bit:  $\hat{s} \leftarrow 1$ 
8:   else
9:     Estimated bit:  $\hat{s} \leftarrow 0$ 
10:  end if
11:  return  $\hat{s}$ 
12: end function
13: function WHITTLE( $Y[k], f_k, \lambda$ )
14:   $l \leftarrow \sum_{k=1}^{N/2-1} \frac{Y_k}{S(f_k, \lambda)} + \ln S(f_k, \lambda)$ 
15:  return  $l$ 
16: end function

```

Considering that $S(f)$ is a slowly varying function, calculating individual periodogram values in (28) is unnecessary because periodogram values can be smoothed by summing over frequency such that

$$\sum_{n=1}^{N/2-1} Y_k \phi(f_k) \simeq \sum_{n=1}^{N/2-1} S(f_k) \phi(f_k), \quad (29)$$

for any smooth function $\phi(f_k)$ [25], [26]. Based on (29), (28) can be simplified as [25]

$$\mathbf{F}^{(ij)} \simeq \sum_{k=1}^{N/2-1} \frac{1}{S^2(f_k)} \frac{\partial S}{\partial \lambda_i} \frac{\partial S}{\partial \lambda_j}, \quad (30)$$

where the derivatives are taken at the true value of the parameters. (30) can also be approximated to integral [25], [26]:

$$\mathbf{F}^{(ij)} \simeq \frac{N\Delta t}{2} \int_0^{\frac{1}{2\Delta t}} \frac{1}{S^2(f)} \frac{\partial S}{\partial \lambda_i} \frac{\partial S}{\partial \lambda_j} df. \quad (31)$$

(31) is a good approximation for a large number of samples such that periodogram values can be approximated as Gaussian by the central limit theorem [27].

MC-Rx decides the transmitted bit by applying the ML decision rule to the estimated concentration of the information molecule, denoted as \hat{c}_m . In the case of FDD, the ML decision threshold is defined as follows:

$$\begin{aligned} \gamma_{fd} = & \frac{1}{\sigma_{\hat{c}_{m|1}}^2 - \sigma_{\hat{c}_{m|0}}^2} \left(\sigma_{\hat{c}_{m|1}}^2 c_{m|0} - \sigma_{\hat{c}_{m|0}}^2 c_{m|1} + \sigma_{\hat{c}_{m|1}} \sigma_{\hat{c}_{m|0}} \right. \\ & \left. \times \sqrt{(c_{m|1} - c_{m|0})^2 + 2(\sigma_{\hat{c}_{m|1}}^2 - \sigma_{\hat{c}_{m|0}}^2) \ln(\sigma_{\hat{c}_{m|1}} / \sigma_{\hat{c}_{m|0}})} \right), \end{aligned} \quad (32)$$

where $\sigma_{\hat{c}_{m|s}}^2$ is the variance and $c_{m|s}$ is the expected value of estimated information molecule when the transmitted bit is $s \in \{0, 1\}$.

The MC-Rx is assumed to know the peak information molecule concentrations for bit-0 and bit-1 at the sampling

time, as expressed by the equation:

$$c_{m|s} = \frac{N_{m|s}}{A_{ch} \sqrt{4\pi D t_d}}. \quad (33)$$

As the MC-Rx does not know the interfering molecule concentration, it computes the decision threshold, γ_{fd} , assuming the absence of interference in the channel. Therefore, the computation of ML decision threshold γ_{fd} relies on the following PSD model for a single type of molecule, i.e., information molecule:

$$S(f, c_m) = 4N_r \zeta^2 \frac{1}{2\pi f + 1/\tau_m} p_b(1 - p_b) + S_f(f), \quad (34)$$

where $\tau_m = 1/(c_m k_m^+ + k_m^-)$ and $p_b = \frac{c_m}{K_{D_m} + c_m}$. Using (34), and (30) for $\lambda = [c_m]$, the variance of estimated information molecule concentration corresponding to the transmitted bit $s \in \{0, 1\}$ is written as [11]

$$\sigma_{\hat{c}_{m|s}}^2 = \frac{1}{\frac{N\Delta t}{2} \int_0^{\frac{1}{2\Delta t}} \frac{1}{S^2(f, c_{m|s})} \left(\frac{\partial S}{\partial c_m} \right)^2 \Big|_{c_m=c_{m|s}} df}. \quad (35)$$

(35) does not give the actual asymptotic variances since MC-Rx estimates the value of c_m based on the model PSD given by (22).

Algorithm 1 outlines the FDD procedure, providing the necessary functions for solving the estimation problem defined by equation (26) and determining the transmitted bit at the receiver. On line 2, the initial concentration values $[c_m^0, c_i^0]$ are obtained by sweeping over sparse concentration values on WHITTLE($Y[k], f_k, \lambda$) and selecting the values that minimize the corresponding function. On line 3, the variable f_k represents the frequencies for which periodogram values are available. On line 4, Newton-Raphson method is used to solve the estimation problem defined in (26) by using WHITTLE($Y[k], f_k, \lambda$) and the initial concentration values $[c_m^0, c_i^0]$ as the starting points. Once the optimal λ^* is found, lines 6-11 execute the thresholding operation on the estimated information molecule concentration \hat{c}_m to determine the transmitted bit.

D. Asymptotic Bit Error Probability

To calculate BEP for FDD, we need the actual values of the variance of estimated information molecule concentration corresponding to $s = 0$ and $s = 1$, i.e., $\sigma_{\hat{c}_{m|s}}^2$. Using the model PSD $S(f, \lambda)$ given by (22), and (30) with $\lambda = [c_m, c_i]$, the variance can be expressed as

$$\sigma_{\hat{c}_{m|s}}^2 = (\mathbf{F}_s(\lambda))_{(11)}^{-1}, \quad (36)$$

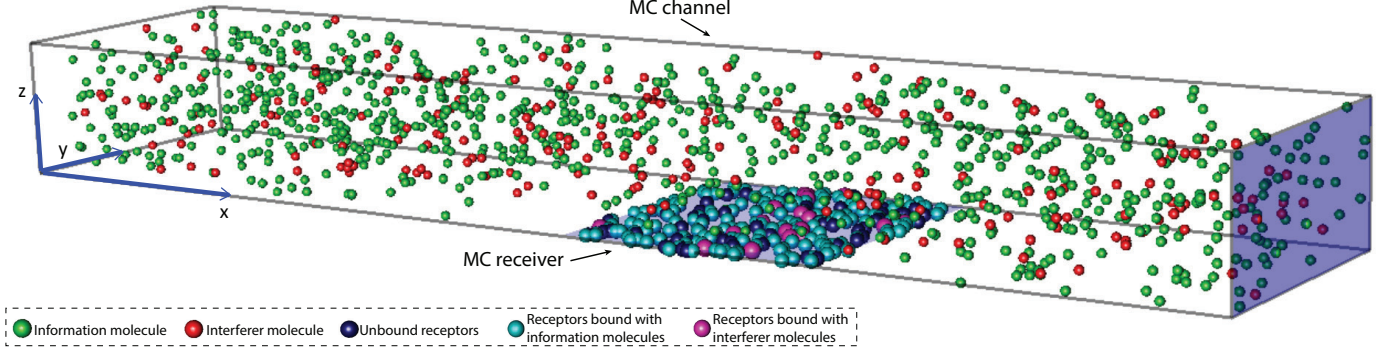


Fig. 2: Snapshot of the Smoldyn simulation illustrating the MC system. The parameters have been adjusted for illustrative purposes. Thus, this representation is not to scale.

where \mathbf{F}_s 's elements are:

$$\begin{aligned} \mathbf{F}_{s(11)} &= \frac{N\Delta t}{2} \int_0^{\frac{1}{2\Delta t}} \frac{1}{S^2(f, (c_{m|s}, \mu_{c_i}))} \left(\frac{\partial S}{\partial c_m} \right)^2 \Big|_{\substack{c_m=c_{m|s} \\ c_i=\mu_{c_i}}} df \\ \mathbf{F}_{s(22)} &= \frac{N\Delta t}{2} \int_0^{\frac{1}{2\Delta t}} \frac{1}{S^2(f, (c_{m|s}, \mu_{c_i}))} \left(\frac{\partial S}{\partial c_i} \right)^2 \Big|_{\substack{c_m=c_{m|s} \\ c_i=\mu_{c_i}}} df, \\ \mathbf{F}_{s(12),(21)} &= \frac{N\Delta t}{2} \int_0^{\frac{1}{2\Delta t}} \frac{1}{S^2(f, (c_{m|s}, \mu_{c_i}))} \left(\frac{\partial S}{\partial c_m} \right) \left(\frac{\partial S}{\partial c_i} \right) \Big|_{\substack{c_m=c_{m|s} \\ c_i=\mu_{c_i}}} df. \end{aligned} \quad (37)$$

As a result, BEP for FDD can be written as

$$P_e^{FDD} = \frac{1}{4} \operatorname{erfc} \left(\frac{\gamma fd - c_{m|0}}{\sqrt{2\sigma_{\hat{c}_{m|0}}^2}} \right) + \frac{1}{4} \operatorname{erfc} \left(\frac{c_{m|1} - \gamma fd}{\sqrt{2\sigma_{\hat{c}_{m|1}}^2}} \right). \quad (38)$$

Here, it should be noted that (38) is an asymptotic expression based on the Gaussian distribution assumption in Sec. IV-C.

V. SIMULATION OF THE SYSTEM

In this section, we detailed the simulation process used to validate our FDD technique. Specifically, we conducted Monte Carlo simulations to compare the theoretical results obtained by the analytical expressions derived in Sections III and IV and the results obtained through particle-based stochastic simulations. For the latter, we used Smoldyn [28]. The simulation algorithms were implemented in MATLAB, and parallelized CPU cores were used for reasonable computation times.

A. Particle-based Stochastic Simulations

We used the open-source particle-based spatial stochastic simulator, *Smoldyn*, to simulate the system. Its capability to capture stochastic events at a molecular level, such as diffusion and receptor binding/unbinding, fits our purpose [28]. As illustrated in Fig. 2, we created a straight microfluidic channel with a rectangular cross-section. The receptors are located in a specific region on the channel bed, indicating the position of the MC receiver.

B. Simulation Parameters

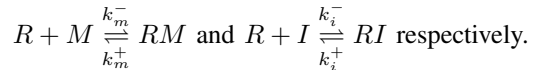
The simulation time step is an important parameter that affects the accuracy of Smoldyn. Using shorter time steps generally leads to higher accuracy but slower simulations. When choosing the time step, one consideration is to ensure it is significantly shorter than the characteristic time scale of any reaction in the system. For the reactions described by (12), the characteristic times or time constants can be obtained from the matrix $\mathbf{\Omega}$ defined by (18), as follows:

$$\tau_{c_{1,2}} = -1/\lambda_{c_{1,2}}, \quad (39)$$

where $\lambda_{c_{1,2}}$ corresponds to the eigenvalues of $\mathbf{\Omega}$. These time constants only depend on the kinetics of the reactions and the concentrations of the information and interferer molecules. Therefore, given the transmitted bit s , the characteristic times (39) can be expanded as

$$\tau_{c_{1,2|s}} = \frac{2}{\left[\frac{1}{\tau_{m|s}} + \frac{1}{\tau_i} \pm \sqrt{\left(\frac{1}{\tau_{m|s}} - \frac{1}{\tau_i} \right)^2 + 4k_m^+ c_{m|s} k_i^+ c_i} \right]}, \quad (40)$$

where $\tau_{m|s} = 1/(c_{m|s}k_m^+ + k_m^-)$, $\tau_i = 1/(c_i k_i^+ + k_i^-)$ correspond to the characteristic times of the independent reactions



Considering the system parameters summarized in Table I, we have chosen the simulation time step as $\Delta t_s = 0.0025$ s. This choice represents a good compromise between accuracy and total execution time. Further reducing the time step can significantly increase the simulation time, posing a challenge for repeated experiments.

The noise PSD, given by equations (20)-(22), can be described as a superposition of Lorentzian spectral profiles. When they are not masked, the corner frequencies of these Lorentzian profiles are defined by the characteristic frequencies, which can be expressed in terms of characteristic times as $f_{c_{1,2|s}} = 1/(2\pi\tau_{c_{1,2|s}})$. When these frequencies are not masked, they can be identified by locating the peaks of the noise PSD multiplied by the corresponding frequency, as illustrated in Fig. 3a. Since the PSD exhibits a profile defined by its characteristic frequencies, which contain information about the equilibrium concentration of the information molecules within

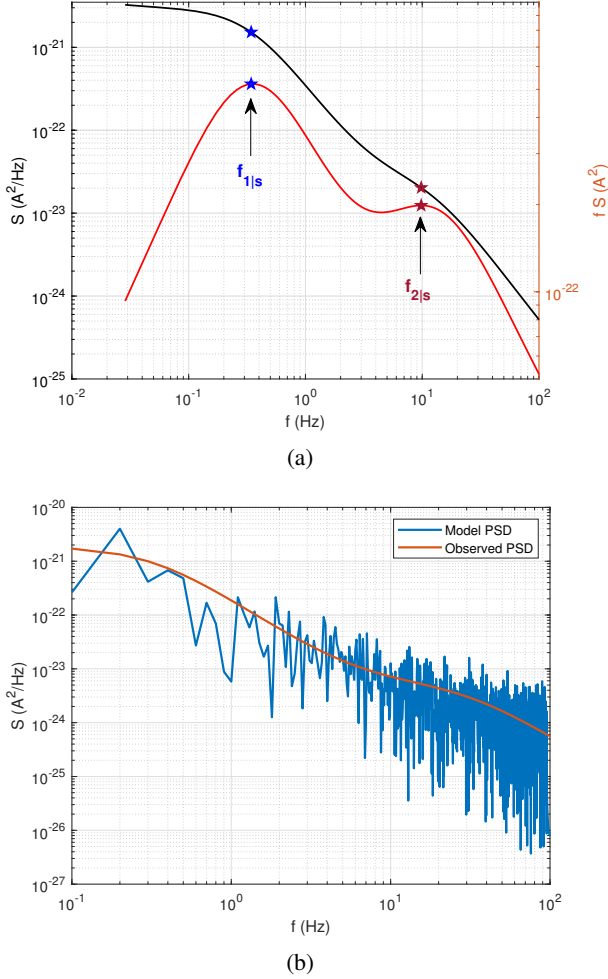


Fig. 3: (a) Characteristic frequencies highlighted on the graph of the S multiplied by frequency f , where S is the theoretical PSD of noise. (b) Model PSD generated with estimated molecule concentrations and the observed PSD (periodogram) generated with the Smoldyn data.

the sampling window, it is crucial to resolve these characteristic frequencies to extract the relevant information accurately. In this regard, the sampling period Δt is a relevant parameter. The maximum observable frequency can be determined by $f_{c_{\max}} = \frac{1}{2\Delta t}$. When a characteristic frequency exceeds this limit, certain portion of the information can be lost.

C. Monte Carlo Simulations

The Monte Carlo algorithm used to validate the BEP performance of FDD is described in Algorithm 2. In each iteration (line 6-19), representing the transmission of a random bit s in the microfluidic channel, the procedure is as follows.

Based on the equilibrium assumption explained in Sec. II, the information molecule concentration $c_{m|s}$ and interferer concentration c_i are assumed to remain constant within the sampling window. Therefore, the corresponding information concentration $c_{m|s}$ for the generated bit s and the interferer concentration c_i generated from a log-normal distribution

Algorithm 2 Monte Carlo Simulation

- 1: **Initialize:** TDD error $e_t \leftarrow 0$, FDD error $e_f \leftarrow 0$
- 2: Generate a *bitstream* consisting of M bits
- 3: Find decision threshold for TDD γ_{td}
- 4: Find decision threshold for FDD γ_{fd}
- 5: **for** each bit s in *bitstream* **do**
- 6: Compute information concentrations $c_{m|s}$ with (3)
- 7: Generate interferer concentration $c_i \sim \log \mathcal{N}(a, b)$
- 8: Run Smoldyn. Wait until equilibrium.
- 9: Record N samples from the number of bound receptors $n_B[k]$ for $k = 1, \dots, N$ with sampling period Δt
- 10: Generate $1/f$ noise samples in the time domain $n_{1/f}[k]$ for $k = 1, \dots, N$
- 11: Convert to electrical output $I_b[k] \leftarrow n_{1/f}[k] + \zeta n_B[k]$ for $k = 1, \dots, N$
- 12: Take one sample, denoted as I_1 , from $I_b[k]$
- 13: $\hat{s}_t \leftarrow \text{TIMEDETECTION}(\gamma_{td}, I_1)$
- 14: If $\hat{s}_t \neq s$, increment e_t by 1.
- 15: Isolate the noise, denoted as $\Delta I_b[k]$, from $I_b[k]$
- 16: Apply low pass filter to $\Delta I_b[k]$ to obtain $\Delta I_{b_f}[k]$
- 17: Compute the periodogram $Y[m]$ for $\Delta I_{b_f}[k]$, for $m = 1, \dots, \frac{N}{2} - 1$ and sampling period Δt
- 18: $\hat{s}_f \leftarrow \text{FREQUENCYDETECTION}(Y[m], N, \Delta t, \gamma_{fd})$
- 19: If $\hat{s}_f \neq s$, increment e_f by 1.
- 20: **end for**
- 21: Compute BEP for TDD: $P_e^{TDD} \leftarrow e_t/M$
- 22: Compute BEP for FDD: $P_e^{FDD} \leftarrow e_f/M$
- 23: **function** TIMEDETECTION(γ_{td}, I_1)
- 24: **if** $I_1 > \gamma_{td}$
- 25: Estimated bit: $\hat{s} \leftarrow 1$
- 26: **else**
- 27: Estimated bit: $\hat{s} \leftarrow 0$
- 28: **end if**
- 29: **return** \hat{s}
- 30: **end function**

represent the concentrations at the sampling time. With these initial values, the Smoldyn simulation is run for a time duration sufficient for the binding reactions to reach equilibrium. Once equilibrium is attained, time samples are taken from the output of the Smoldyn (line 9), where the output corresponds to the number of bound receptors. The collected time samples are then scaled and combined with $1/f$ noise to simulate the transduction process of the bioFET, resulting in the electrical output denoted as $I_b[k]$.

To simulate the $1/f$ noise in the time domain, we employed the FIR filtering method described in [29], which involves filtering white Gaussian noise in the frequency domain using an FIR filter with a $1/f$ passband and subsequently performing an inverse Fourier transform to obtain the $1/f$ noise sequence. The approximate noise variance σ_f^2 is computed based on the expression given in Equation (6), with the parameter values specified in Table I.

As stated in line 12, a single sample is taken from the middle of the electrical output $I_b[k]$ for TDD. For FDD, the base signal is removed from the electrical output $I_b[k]$ to isolate

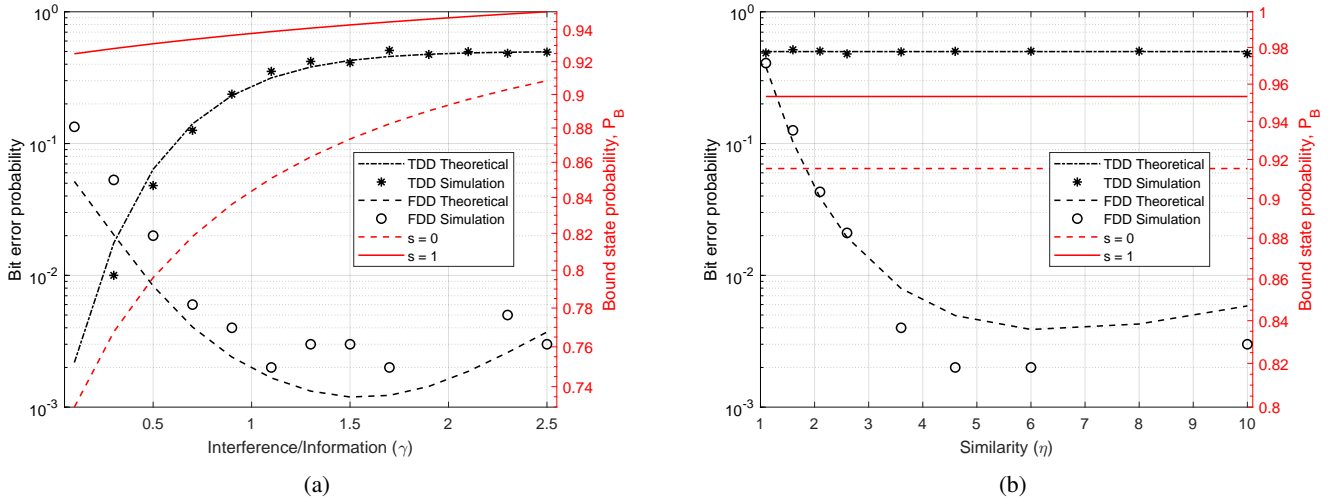


Fig. 4: BEP for varying (a) information to interference ratio γ and (b) similarity η .

the noise component, $\Delta I_b[k]$. Additionally, considering that samples are taken within a finite sampling window, distortions near the Nyquist frequency in the PSD are inevitable due to the aliasing. Therefore, a low-pass filter with a passband near the Nyquist frequency is applied to the sampled noise to mitigate this distortion, as outlined in line 16. This filtering step helps reduce outliers that could affect the accuracy of the MLE. Then, periodogram PSD is computed using an N-point FFT of the filtered noise samples. No further processing is performed on the noise signal or the estimated PSD before the MLE to avoid introducing statistical distortion, which can result in erroneous parameter predictions. Finally, the MLE is performed by MATLAB's *fminunc* solver [30], which uses the quasi-Newton algorithm. The solver can find the solution within a few iterations in this specific scenario. Finally, BEP for TDD and FDD are computed as described by line 20-21.

Fig. 3b depicts the model noise PSD generated using the MLE estimated information and interferer concentration pair, $[\hat{c}_m|s, \hat{c}_i]$, and the periodogram estimate of the observed noise PSD obtained by using the data from the Smoldyn.

VI. PERFORMANCE EVALUATION

In this section, we analyze the performance of FDD and TDD in terms of BEP. The default values of the system parameters are given in Table I, with the reaction rates adopted from [11]. Unless stated otherwise, the default parameter values are used in the rest of the paper.

It can be observed that the simulation results can deviate from the theoretical results due to the inherent nature of Monte Carlo simulations. Especially when dealing with high concentration values (high signal variance), Monte Carlo simulations can require a large number of iterations to converge, potentially leading to excessive simulation times when using Smoldyn. Therefore, to maintain a compromise between convergence and simulation times, we chose moderate number of iterations (1000) for the Monte Carlo simulations.

A. Effect of Interference on BEP

In the initial analysis, we examine the impact of interference strength on the BEP performance of both TDD and FDD. To investigate this, we introduce a tuning parameter γ , which determines the mean interferer concentration μ_{c_i} as $\mu_{c_i} = \gamma \cdot c_{m|s=1}$. The results, as depicted in Fig. 4a, show that FDD outperforms TDD, except in cases where the interferer concentration is significantly lower than the concentration of information molecules as shown in Fig. 4a. As the interferer concentration increases, the performance of TDD deteriorates. This degradation occurs because the increasing number of bound receptors becomes occupied by the interfering molecules, leading to saturation of the receiver, thereby causing increase in the error probability. On the other hand, the performance of FDD improves with increasing interferer concentration up to a certain point, after which it starts to degrade.

TABLE I: Default Values of System Parameters

Temperature (T)	300 K
Microfluidic channel height (h_{ch}), width (w_{ch})	5 μm , 10 μm
Average flow velocity (u)	10 $\mu\text{m/s}$
Distance of Rx's center position to Tx (x_R)	1 mm
Ionic concentration of medium (c_{ion})	30 mol/m ³
Relative permittivity of medium (ϵ/ϵ_0)	80
Intrinsic diffusion coefficient (D_0)	2×10^{-11} m ² /s
Binding rate of information and interferer molecules (k_m^+, k_i^+)	4×10^{-17} m ³ /s
Unbinding rate of information molecules (k_m^-)	2 s^{-1}
Unbinding rate of interferers (k_i^-)	8 s^{-1}
Average # of electrons in a ligand (N_{e-})	3
Number of independent receptors (N_r)	120
Effective length of a surface receptor (r)	2 nm
Transconductance of graphene bioFET (g)	1.9044×10^{-4} A/V
Width of graphene in transistor (l_{gr})	10 μm
Quant. capacitance of graphene per unit area (c_q)	2×10^{-2} F m ⁻²
# of transmitted ligands for $s = 0, 1$ ($N_{m s}$)	$[1, 5] \times 10^3$
# of noise samples (N)	700
Sampling period (Δt)	0.005 s
Mean interference to information concentration ratio ($\gamma = \mu_{c_i}/c_{m s=1}$)	0.7
Interference mean/std ratio (μ_{c_i}/σ_{c_i})	10
Power of 1/f noise at 1 Hz ($S_{f1\text{Hz}}$)	10^{-23} A ² /Hz
Noise exponent for 1/f noise (β)	1
Lower frequency limit for 1/f noise (f_L)	10^{-8}
Upper frequency limit for 1/f noise (f_H)	10^7

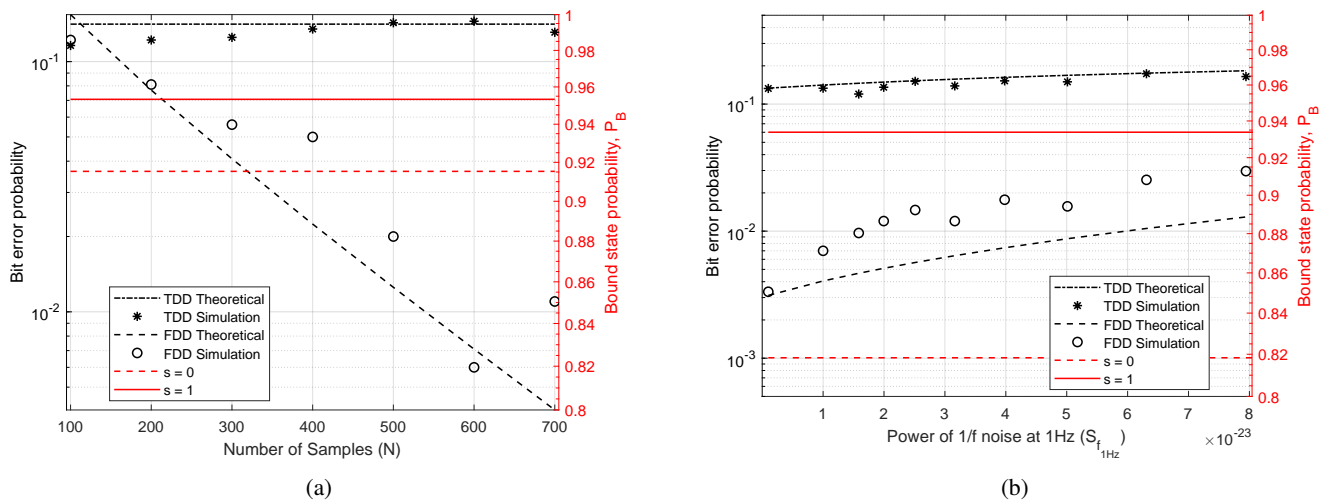


Fig. 5: BEP for varying (a) number of samples (b) power of $1/f$ noise at 1 Hz.

Considering that the characteristic frequencies are influenced by both the concentration and affinities of the molecules, the effect of interference is initially indistinguishable in the PSD. This is because the concentration of interfering molecules is initially lower, which results in the individual Lorentzian PSD attributed to interfering molecules being overshadowed by that of the information-carrying molecules. However, as the concentration of interfering molecules increases, its impact on the combined PSD becomes more pronounced, allowing for a more accurate estimation of concentrations and, consequently, reduced error probabilities. Nevertheless, beyond a particular concentration of interfering molecules, the Lorentzian PSD attributed to the information-carrying molecules is overshadowed, increasing error probabilities.

B. Effect of Similarity on BEP

We also consider the effect of the affinity ratio between the information and interferer molecules, which we refer as the similarity parameter and define as $\eta = \frac{K_{D_i}}{K_{D_m}}$. To observe the direct effect of the similarity, we keep the bound state probabilities constant by scaling the mean interferer concentration, μ_{c_i} , by η . As expected, TDD is not affected by the similarity parameter, as shown in Figure 4b. This occurs because the TDD method relies on the total bound state probability p_{b_s} , which remains constant in this case, thereby not affected by changes in similarity. On the other hand, BEP for FDD exhibits an interesting behavior. BEP improves as the similarity parameter η increases, indicating that the information and interfering molecules become dissimilar. However, beyond a specific value of the similarity parameter, BEP starts to degrade. This trend can be explained as follows: When the similarity parameter η is low, indicating high similarity between the information and interfering molecules, FDD cannot distinguish between these two types of molecules based on their affinities. This is because any noticeable distinction is not reflected in the spectrum. For example, when the similarity parameter η is close to 1, the noise PSD appears as a single Lorentzian profile, thereby obscuring the Lorentzian profile associated with the reaction RM in the spectrum. As the similarity increases,

it becomes more visible that PSD is the superposition of two Lorentzian profiles, and the characteristic frequencies $f_{1|s}$ and $f_{2|s}$ are more distinguishable. However, once the similarity goes beyond the point where $f_{1|s}$ and $f_{2|s}$ are most distinguishable, the PSD becomes less informative about the concentration of information $c_{m|s}$. This occurs because interference becomes the dominant factor on the profile of the PSD, and the variations in $c_{m|s}$ have a lesser impact on the PSD. As a result, the PSD becomes less informative about the information concentration, $c_{m|s}$, increasing the error probability.

C. Effect of Number of Samples on BEP

The BEP performance is further analyzed for the number of time samples N . As depicted in Fig. 5a, it is observed that the performance of FDD improves as the number of samples increases. This outcome aligns with expectations, as a larger number of samples leads to a decrease in the variance of the estimated information molecule concentration, $\sigma_{\hat{c}_{m|s}}^2$. The reduction in variance results in more accurate estimation as the error on the estimated parameter follows $\sigma_{\hat{c}_{m|s}} \propto \sqrt{(\mathbf{F}_s)_{(11)}^{-1}/N}$. Consequently, more samples lead to a decrease in the BEP. On the other hand, the performance of TDD remains unaffected by the number of samples, as the receiver only takes one sample, typically from the middle of the signal within the sampling window.

D. Effect of $1/f$ noise on BEP

We also simulate the BEP performance of FDD and TDD under varying $1/f$ noise power (at 1 Hz), as depicted in Fig. 5b. To better observe the performance trend, a similarity value of $\eta = 3$ is chosen for this case. The results show that $1/f$ noise affects the performance of both TDD and FDD. Additionally, it can be observed that the performance of FDD is more sensitive to changes in the $1/f$ noise levels compared to TDD. Since $1/f$ noise is directly additive across the entire spectrum, increasing the $1/f$ noise level reduces the FDD performance by potentially masking critical frequencies under the background $1/f$ noise.

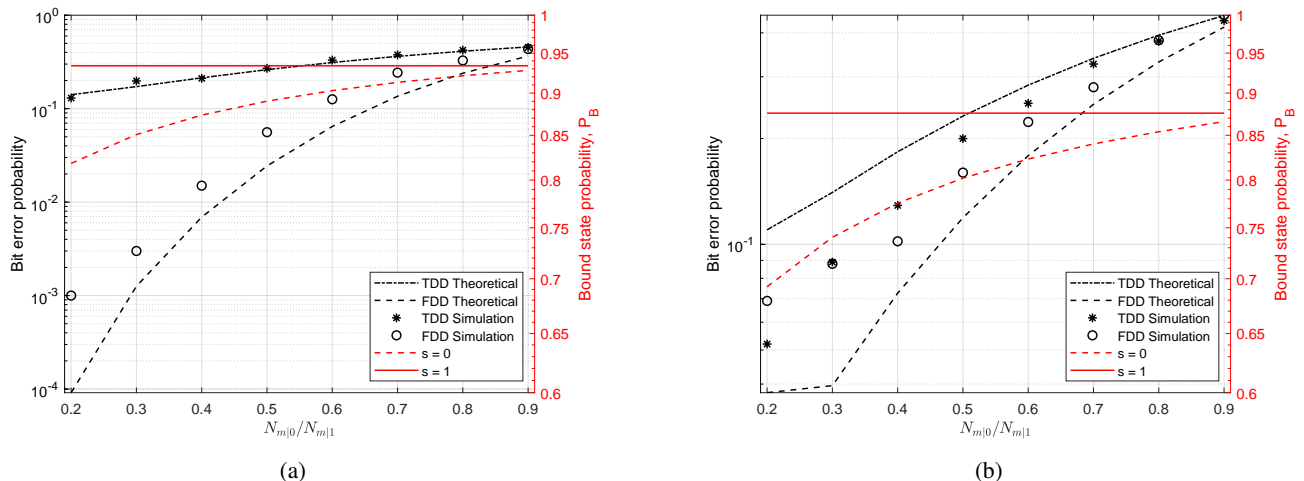


Fig. 6: BEP for varying bit-0/bit-1 concentration ratio when the MC-Rx is (a) near saturation, and (b) in a non-saturation state.

E. Effect of Bit-0/Bit-1 concentration ratio on BEP

We further explored the impact of the ratio of concentrations for bit-0 and bit-1, denoted as $N_{m|0}/N_{m|1}$, on the BEP. As depicted in Fig. 6a, it becomes apparent that the detection performances of both TDD and FDD methods experience a decline when the concentration values become closer.

In Fig. 6a, the MC-Rx is observed in near saturation, implying a high level of receptor occupancy. Comparing the performance in Fig. 6a with the result shown in Fig. 6b, which corresponds to a case of lower bound state probabilities, a noticeable performance decline can be observed in the latter.

These results suggest that the FDD method is more effective when the receptor occupancy at the MC-Rx is higher. This property could be advantageous, as it aligns more closely with the typical conditions encountered in MC, wherein the receiver is commonly expected to operate near saturation most of the time due to the remaining molecules from previous transmissions or interferers.

VII. CONCLUSION

In this paper, we propose a frequency-domain detection method for the bioFET-based molecular communication receivers. The method leverages the receptor cross-reactivity to different ligands and utilizes the output noise power spectral density to detect the transmitted bit. We derived the bit error probability for frequency domain and one-shot time domain detection methods by considering a microfluidic channel where a single type of interfering molecules is present. We employed a particle-based spatial simulator to validate our theoretical derivations for bit error probabilities. Our analysis indicates a significant performance advantage of the proposed frequency-domain detection method over the time-domain detection method, especially in scenarios with high interference in the channel. This characteristic of the frequency-domain detection can be helpful since it can be applicable to practical conditions encountered in molecular communication, where receivers often operate close to saturation at high data transmission rates due to the presence of remaining molecules from previous transmissions or interference.

REFERENCES

- [1] O. B. Akan, H. Ramezani, T. Khan, N. A. Abbasi, and M. Kuscü, "Fundamentals of molecular information and communication science," *Proc. IEEE*, vol. 105, no. 2, pp. 306–318, 2016.
- [2] I. F. Akyildiz, M. Ghovanloo, U. Guler, T. Ozkaya-Ahmadov, A. F. Sarioglu, and B. D. Unluturk, "Panacea: An internet of bio-nanotechnology application for early detection and mitigation of infectious diseases," *IEEE Access*, vol. 8, pp. 140 512–140 523, 2020.
- [3] C. Koca, M. Civas, S. M. Sahin, O. Ergonul, and O. B. Akan, "Molecular communication theoretical modeling and analysis of sars-cov2 transmission in human respiratory system," *IEEE Transactions on Molecular, Biological and Multi-Scale Communications*, vol. 7, no. 3, pp. 153–164, 2021.
- [4] D. P. Martins, M. T. Barros, B. J. O'Sullivan, I. Seymour, A. O'Riordan, L. Coffey, J. B. Sweeney, and S. Balasubramaniam, "Microfluidic-based bacterial molecular computing on a chip," *IEEE Sensors Journal*, vol. 22, no. 17, pp. 16 772–16 784, 2022.
- [5] M. Kuscü, E. Dinc, B. A. Bilgin, H. Ramezani, and O. B. Akan, "Transmitter and receiver architectures for molecular communications: A survey on physical design with modulation, coding, and detection techniques," *Proceedings of the IEEE*, vol. 107, no. 7, pp. 1302–1341, 2019.
- [6] M. Kuscü, H. Ramezani, E. Dinc, S. Akhavan, and O. B. Akan, "Fabrication and microfluidic analysis of graphene-based molecular communication receiver for internet of nano things (ion)," *Scientific reports*, vol. 11, no. 1, pp. 1–20, 2021.
- [7] T. Mora, "Physical limit to concentration sensing amid spurious ligands," *Physical review letters*, vol. 115, no. 3, p. 038102, 2015.
- [8] C. Koca, M. Civas, and O. Akan, "Narrow escape problem in synaptic molecular communications," in *Proceedings of the 9th ACM International Conference on Nanoscale Computing and Communication*, 2022, pp. 1–7.
- [9] M. Kuscü and O. B. Akan, "Channel sensing in molecular communications with single type of ligand receptors," *IEEE Transactions on Communications*, vol. 67, no. 10, pp. 6868–6884, 2019.
- [10] C. Koca and O. B. Akan, "Channel clearance by perfectly absorbing boundaries in synaptic molecular communications," *IEEE Access*, vol. 10, pp. 121 480–121 493, 2022.
- [11] M. Kuscü and O. B. Akan, "Detection in molecular communications with ligand receptors under molecular interference," *Digital Signal Processing*, vol. 124, p. 103186, 2022.
- [12] L. J. Mele, P. Palestri, and L. Selmi, "General model and equivalent circuit for the chemical noise spectrum associated to surface charge fluctuation in potentiometric sensors," *IEEE Sensors Journal*, vol. 21, no. 5, pp. 6258–6269, 2020.
- [13] M. Civas, A. Abdali, M. Kuscü, and O. B. Akan, "Frequency-domain detection for molecular communications," *Proceedings of IEEE ICC 2023*, 2023.
- [14] M. Civas, M. Kuscü, O. Cetinkaya, B. E. Ortlek, and O. B. Akan, "Graphene and related materials for the internet of bio-nano things," *APL Materials*, vol. 11, no. 8, p. 080901, 2023.

- [15] E. Limpert, W. A. Stahel, and M. Abbt, "Log-normal distributions across the sciences: keys and clues: on the charms of statistics, and how mechanical models resembling gambling machines offer a link to a handy way to characterize log-normal distributions, which can provide deeper insight into variability and probability—normal or log-normal: that is the question," *BioScience*, vol. 51, no. 5, pp. 341–352, 2001.
- [16] M. Kuscü and O. B. Akan, "Modeling convection-diffusion-reaction systems for microfluidic molecular communications with surface-based receivers in internet of bio-nano things," *PloS one*, vol. 13, no. 2, p. e0192202, 2018.
- [17] A. O. Bicen and I. F. Akyildiz, "System-theoretic analysis and least-squares design of microfluidic channels for flow-induced molecular communication," *IEEE Transactions on Signal Processing*, vol. 61, no. 20, pp. 5000–5013, 2013.
- [18] M. Kuscü and O. B. Akan, "Modeling and analysis of sinw fet-based molecular communication receiver," *IEEE Transactions on Communications*, vol. 64, no. 9, pp. 3708–3721, 2016.
- [19] I. Heller, S. Chatoor, J. Mannik, M. A. Zevenbergen, J. B. Oostinga, A. F. Morpurgo, C. Dekker, and S. G. Lemay, "Charge noise in graphene transistors," *Nano letters*, vol. 10, no. 5, pp. 1563–1567, 2010.
- [20] J. Mucksch, P. Blumhardt, M. T. Strauss, E. P. Petrov, R. Jungmann, and P. Schwille, "Quantifying reversible surface binding via surface-integrated fluorescence correlation spectroscopy," *Nano Letters*, vol. 18, no. 5, pp. 3185–3192, 2018.
- [21] S. Vaughan, "A bayesian test for periodic signals in red noise," *Monthly Notices of the Royal Astronomical Society*, vol. 402, no. 1, pp. 307–320, 2010.
- [22] D. Barret and S. Vaughan, "Maximum likelihood fitting of x-ray power density spectra: application to high-frequency quasi-periodic oscillations from the neutron star x-ray binary 4u1608-522," *The Astrophysical Journal*, vol. 746, no. 2, p. 131, 2012.
- [23] A. M. Sykulski, S. C. Olhede, A. P. Guillaumin, J. M. Lilly, and J. J. Early, "The debiased whittle likelihood," *Biometrika*, vol. 106, no. 2, pp. 251–266, 2019.
- [24] E. R. Anderson, T. L. Duvall Jr, and S. M. Jefferies, "Modeling of solar oscillation power spectra," *The Astrophysical Journal*, vol. 364, pp. 699–705, 1990.
- [25] T. Toutain and T. Appourchaux, "Maximum likelihood estimators: An application to the estimation of the precision of helioseismic measurements," *Astronomy and Astrophysics*, vol. 289, pp. 649–658, 1994.
- [26] M. Levin, "Power spectrum parameter estimation," *IEEE Transactions on Information Theory*, vol. 11, no. 1, pp. 100–107, 1965.
- [27] K. Libbrecht, "On the ultimate accuracy of solar oscillation frequency measurements," *The Astrophysical Journal*, vol. 387, pp. 712–714, 1992.
- [28] S. S. Andrews, "Smoldyn: particle-based simulation with rule-based modeling, improved molecular interaction and a library interface," *Bioinformatics*, vol. 33, no. 5, pp. 710–717, 2017.
- [29] N. J. Kasdin, "Discrete simulation of colored noise and stochastic processes and $1/f$ power law noise generation," *Proceedings of the IEEE*, vol. 83, no. 5, pp. 802–827, 1995.
- [30] T. M. Inc., "Optimization toolbox version: 9.2 (r2021b)," Natick, Massachusetts, United States, 2022. [Online]. Available: <https://www.mathworks.com>